Preparation by electrophoretic deposition of molybdenum iodide cluster-based functional nanostructured photoelectrodes for solar cells

A. Renaud, T.K.N. Nguyen, F. Grasset, M. Raissi, V. Guillon, F. Delabrouille, N. Dumait, P.-Y. Jouan, L. Cario, S. Jobic, et al.

Preparation by Electrophoretic Deposition of Molybdenum Iodide Cluster-based Functional Nanostructured Photoelectrodes for Solar Cells

A. Renaud,[a]* T. K. N. Nguyen,[b,c] F. Grasset,[b,c] M. Raissi,[d] V. Guillon,[e] F. Delabrouille,[e] N. Dumait,[a] P.-Y. Jouan,[f] L. Cario,[f] S. Jobic,[f] Y. Pellegrin,[d] F. Odobel,[d] S. Cordier,[a] T. Uchikoshi [b,c]

[a]Univ Rennes, CNRS, ISCR – UMR 6226, F-35000 Rennes, France. Email: adele.renaud@univ-rennes1.fr

[b]CNRS - Saint-Gobain - NIMS, UMI 3629, Laboratory for Innovative Key Materials and Structures (LINK), National Institute for Materials Science, 1-1 Namiki, 305-0044, Tsukuba, Japan.

[c]National Institute for Materials Science, RCFM, 1–1 Namiki, Tsukuba, Ibaraki 305–0044, Japan

[d]Laboratoire de Chimie et Interdisciplinarité : Synthèse, Analyse, Modélisation (CEISAM), Université de Nantes, 2 rue de la Houssinière, BP 92208, 44322 Nantes Cedex 3, France

[e]EDF R&D, avenue des Renardières, 77818 Moret-sur-loing, France

[f]Institut des Matériaux Jean Rouxel, Université de Nantes, CNRS, 2 rue de la Houssinière, 44322 Nantes cedex 3, France

Abstract

This work explores the potentiality of Mo_6 clusters as new inorganic sensitizers with amphoteric properties for photoelectronic applications being non-toxic and stable. It reports on the design of photoelectrodes by electrophoretic deposition (EPD) of molybdenum octahedral metal cluster iodide (CMI) onto mesoporous TiO_2 and NiO layers before being deposited on FTO (i. e. CMI@TSO@FTO, TSO = TiO_2 or NiO). Indeed, the low-cost, low-waste and industrially scalable EPD method has allowed for the achievement of transparent,

1

homogeneous orange/red $[Mo_6I^i_8]^{4+}$ cluster core-based films, and appears suitable for the sensitization of TiO_2- and NiO-based electrodes of n- and p-type solar cells inspired from dye-sensitized solar cells (DSSCs). First, the EPD process was optimized by the direct deposition of CMI onto an FTO substrate (CMI@FTO) leading to the realization of highly transparent colored films. Second, strongly colored CMI@TSO@FTO photoelectrodes were achieved and integrated into solar cell devices. Hence, compared to the classical soaking method, the EPD process significantly improves the quality (i.e., its homogeneity and absorption properties) of the photoelectrodes, leading consequently to much better photovoltaic performances.

Keywords: molybdenum, metallic cluster, electrophoretic deposition, photoelectrodes, thin film, solar cells.

1. Introduction

In a global context of serious environmental problems and increasing of energy consumption, photoelectrochemical devices are widely investigated for the purpose of energy conversion.[1,2] Indeed, photovoltaic cells, such as dye-sensitized solar cells (DSSCs),[1,3-9] and photocatalytic systems for hydrogen production, like dye-sensitized photoelectrochemical cells (DS-PECs) [10-13] have been, for more than two decades, the source of extensive research. Typically, these types of cells consist of a photoanode (photocathode), which is composed of nanostructured films with n-type (p-type) semiconductors (SC) that are connected to a platinum counter-electrode, or of tandem cells that are built upon the assembly of a photoanode and a photocathode. Transparent semiconducting oxides (TSO), such as TiO_2,[1-7,10-13] ZnO,[14-17] and WO_3[18-21] for n-type semiconductors, or NiO,[8,12,22-24] copper oxides,[25-29] and delafossite compounds[9,26,30-33] for p-type semiconductors, are widely studied as photoelectrode materials for the following reasons: their intrinsic optical and electronic properties, their stability towards photocorrosion and their aptitude for nanostructuration. So

far, due to efficiency reasons, TiO_2 is the most prominently used material for energy conversion. In DSSCs, as well as in DS-PECs, TSOs are associated with a sensitizer (molecular dyes, quantum dots, inorganic pigments, etc.) that absorbs light; once excited, charges are injected in the external circuit of the cell if the electron-hole recombination phenomena at interfaces are minimized.[1,3-15,19-21,23,24,26,28,29,32-34] The mediator redox (typically the I^-/I_3^- redox couple) has an electron shuttle role. It ensures the charge transport between the two electrodes (photoanode/counter-electrode or photoanode/photocathode) in the electrolyte (classically based on a nitrile solvent). Most of the current research concerning electrolytes is focused on the improvement of long-term stability and the safety of DSSCs through the replacement of the liquid organic solvent-based electrolyte with an aqueous electrolyte,[35] ionic liquids,[36,37] polymer gels[37-39] or a membrane,[40,41] solid hole transporting materials (HTMs),[42] etc. In this context, this work aims to investigate, with an exploratory approach, new amphoteric non-toxic and stable sensitizers in order to develop new functionalized nanostructured surfaces that exhibit photo-induced properties. This paper will focus exclusively on DSSCs as a photoelectrochemical application. Indeed, we recently demonstrated the potential interest of inorganic octahedral transition metal clusters as a new class of amphoteric light harvesters in photovoltaic cells inspired from DSSCs.[43] Our investigation opened the door to the integration of these octahedral transition metal clusters as a new non-toxic absorber in all inorganic solar cells inspired from lead-halide perovskite solar cells. Octahedral clusters are 1 nm sized inorganic moieties that consist of six metal atoms connected by metal-metal bonds which form a face-capped or edge-bridged octahedron by 14 or 18 non-metal atoms, respectively, called ligands. The face-capped $[(M_6L^i_8)L^a_6]^{n-}$ clusters are composed of eight face capping inner ligands (L^i, L = halogens or chalcogens) and six apical ligands (L^a = halogens, OH^-, H_2O, CN^-, etc.) (depicted in Figure 1a) while the edge-bridged $[(M_6L^i_{12})L^a_6]^{n+/-}$ ones have twelve inner ligands (L^i = halogens) and six apical ligands

3

(L^a = halogens, OH^-, H_2O, etc.). These cluster units are associated with inorganic or organic counter-ions (alkali cation, quaternary ammonium, etc.) in the solid state. The terminal apical ligands are labile and can easily be exchanged in a solution, while the inner ligands have strong interactions with the octahedral cluster. The chemical nature of L^i and L^a influences the crystal and electronic structures which induce various intrinsic optical and electronic properties. The edge-bridged $[(M_6L^i_{12})L^a_6]^{n+/-}$ units exhibit particularly interesting physicochemical behaviors related to a wide variety of long-range structural arrangements,[44-29] several possible oxidation states of the cluster units and an ability to strongly absorb light in the UV-vis-NIR.[50-52] This opens up an avenue for potential applications in catalysis,[53] biology,[54-57] energy saving applications,[51,52] etc. Much attention is paid to the face-capped $[(M_6L^i_8)L^a_6]^{n-}$ cluster units (L = halogen) due to their strong photoluminescence with a large Stokes shift,[58-61] their intense absorption in the UV-vis domain[43] and their (photo)catalytic properties[62,63] leading to their potential use in energy,[43,64] (photo)catalysis,[63,65] optoelectronic devices[63] and biotechnologies.[67-70] Thus, we have reported the use of the $[Mo_6I_{14}]^{2-}$ cluster as a sensitizer in n- or p-type solar cells with a TiO_2-based photoanode or a NiO-based photocathode, respectively.[43] At that time, the Mo_6-based units were chemisorbed on the TSO surface by soaking the electrode in a cluster-based solution. However, this covering method led either to i) a homogeneous cluster coating with low absorption properties or ii) an inhomogeneous surface with a much pronounced color, but a higher concentration of recombination centers. The highly colored inhomogeneous surfaces are due to the cluster condensation through hydrogen bonding (after anion exchange in solution) under micro-size particles. In order to improve the photoelectrode quality (i.e., the absorption properties and homogeneity of the Mo_6 coating), reinforce the anchoring of the cluster on the electrode surface, and consequently expect higher photovoltaic performances, we have embarked on the functionalization of TSO surfaces with Mo_6 clusters through the electrophoretic deposition

technique (EPD). This was recently successfully applied to the deposition of Mo_6[71-74] or

Ta_6[52,74] clusters on indium-doped tin oxide (ITO) glass substrates from $Cs_2Mo_6Cl_{14}$,

$Cs_2Mo_6Br_{14}$, $Cs_2Mo_6I_8(OOCC_2F_5)_6$, $((n\text{-}C_4H_9)_4N)_2Mo_6Br_{14}$, $K_4Ta_6Br_{18}$ or

$[Ta_6Br_{14}(H_2O)_4].3H_2O$ cluster precursors. We present herein the design by EPD of $[Mo_6I^a_8]^{4+}$-

based photoanodes and photocathodes and its impact on the performances of the photovoltaic

cells.

2. Experimental Section

2.1 Materials and Methods

The chemicals were purchased from Sigma-Aldrich, VWR chemicals, Alfa Aesar and Acros,

and were used as received. The $Cs_2Mo_6I_{14}$ (CMI) powder was synthesized from MoI_2 and CsI

by the solid-state route as previously described.[75]

2.1.1 The EPD Process. The Preparation of CMI Films. Two types of coatings were

prepared: i) a direct deposition of CMI on FTO in order to prepare colored transparent

CMI@FTO films as well as to optimize the EPD process, and ii) a deposition of CMI on TSO

to prepare CMI@TSO@FTO photoelectrodes (TSO = TiO_2 or NiO).

Optimization of the EPD Process and the Preparation of Colored CMI@FTO. Three

types of solvents were tested for the preparation of the EPD solutions: one alcohol (ethanol)

and two ketones (acetone and MEK). Due to the natural condensation of clusters when water

is used (i.e., clusters interact *via* hydrogen bonds after an apical ligand exchange of I^- by OH^-

or H_2O), a deposition in aqueous solutions was not attempted. Actually, a CMI powder was

used as a precursor and was dissolved in acetone (HPLC grade, VWR Chemicals, Figure 1b)

or methyl ethyl ketone (MEK, Alfa Aesar, 99+%) in order to obtain saturated solutions, which

correspond to concentrations of 17 and 10 mM, respectively (i.e., solutions where the

inorganic phase is not totally dissolved). A less concentrated acetone-based solution (7 mM)

was prepared from the saturated one. CMI is not soluble in ethanol. Consequently, the

5

alcohol–based deposition solution was prepared by a solvent exchange with the acetone solution by adding absolute ethanol (Sigma-Aldrich) and the evaporation of acetone with a rotary evaporator. Due to different solubilities, the CMI concentration of this saturated alcoholic solution is lower than the ketone solutions (around 2.5 mM). The EPD setup (Figure 1c) consisted of a clean Fluorine tin oxide (FTO, SnO_2:F, Pilkington TEC8, 8 Ω/sq) substrate used as an anodic electrode and a stainless steel cathode, which were placed face-to-face with 1 cm between the two and connected to a Keithley Model 2450 Series SourceMeter with a carbon tape. Electrodes were immerged into and removed from the EPD solution through the raising and lowering of the lab stand. The FTO substrates were cleaned in three steps of ultrasonication: first, in soapy water, second, in an aqueous solution that was acidified by using a few drops of hydrochloric acid (37%, Sigma-Aldrich), and third in ethanol. Finally, they were air-dried. Once the electrodes were immerged into the EPD solution, a continuous voltage was applied for a fixed time. The applied voltage was stopped once the electrodes were out of the EPD solution and the solvent evaporated. For the optimization step of the EPD process, several EPD experiments were performed using various voltages for deposition times of 5 and 30 s. To do so, we began from the lower to the higher voltage. Orange/red films occurred under an applied voltage ranging from 2 to 40 V.

The Preparation of CMI@TSO@FTO Photoelectrodes. The TiO_2 and NiO mesoporous films on an FTO substrate (TSO electrodes) were prepared according to previously reported protocols.[9,43,75-78] Succinctly, two types of deposition methods, were used for the preparation of electrodes. The doctor blade technique was used for the study of the CMI deposition on the TSO electrodes and the screen-printing technique was chosen for the preparation of the optimized coatings of CMI on a TiO_2- (NiO-) based photoanode (photocathode) for the fabrication of photovoltaic cells. The TiO_2- and NiO-based films on cleaned FTO-coated glass substrates were prepared from a commercial TiO_2 nanoparticles paste (DSL30NRD DyeSol)

and a NiO-based homemade paste that was based on commercial nanoparticles from Inframat©,[43,77,78] respectively. Then, the TiO_2 and NiO electrodes were sintered (in the ambient air at 550 °C for 10 min and 450 °C for 30 min, respectively) to decompose organics and to create electronic percolation pathways. As for the photoanodes prepared for the fabrication of photovoltaic cells, an extra $TiCl_4$ treatment was applied.[76] The CMI deposition on TSO (Figure 1c) was performed from the saturated acetone-based solution (17 mM) by replacing the FTO substrates on the anode side of the EPD setup by TSO electrodes. The deposition protocol is the same as that used for the preparation of the CMI@FTO films. The CMI@TSO@FTO films were prepared under an applied voltage ranging from 2 to 40 V for 30 s.

2.1.2 Solar Cells Fabrication. The solar cells were assembled according to the vacuum back-filling technique.[79] The photoelectrodes were associated with a platinum counter-electrode and the interspace layer was filled back with an electrolyte composed of the iodide/triiodide couple or the tris(4,4'-di(tert-butyl)-2,2'-bipyridine) cobalt(II/III) couple. The composition of the iodide/triiodide electrolyte used in n- or p- DSSCs was slightly different. It consisted of a mixture of 0.05 M I_2, 0.1 M LiI, 0.6 M of 1,2-dimethyl-3-butylimidazolium iodide and 0.5 M (2)4-tertbutylpyridine in acetonitrile for the TiO_2-based DSSCs or a mixture of 0.1 M I_2, 1 M LiI in acetonitrile for the NiO-based DSSCs. The cobalt complex electrolyte was prepared with 0.1 M tris(4,4-bis-tert-butyl-2,2-bipyridine)cobalt(II/III) and 0.1 M $LiClO_4$ in propylene carbonate.[80] Finally, the hole was isolated with a glass disc by using a Surlyn polymer spacer (Dupont, 60 μm). Three n- and p-DSSC cells were prepared from each electrolyte.

2.2 Characterization Techniques. The X-ray powder diffraction (XRPD) data were collected on the CMI bulk and the CMI films at room temperature in a 2θ angle ranging from 5 to 90 ° with a scan speed of 4 °·min^{-1} with a Bruker D8 Advance two-circle diffractometer (θ-2θ Bragg–Brentano mode) using Cu Kα radiation (l = 1.54056 Å) equipped with a Ge(111)

7

monochromator and a Lynx Eye detector. The UV-vis transmission spectra of the transparent films were obtained on a PerkinElmer Lambda 35 spectrophotometer and the CMI powder reflectance spectrum was obtained on a Varian Carry 100 spectrophotometer equipped with a Spectralon reflectance sphere accessory. The optical microscopy images were carried out with a Keyence VHX-1000 microscope. The surface morphology, chemical analyses of photoelectrodes and thickness of coatings on the FTO were investigated by scanning electron microscopy (SEM) using a JEOL JSM 7100 F microscope operating at 10 kV while coupled with an energy dispersive microscope. The NiO and TiO_2 photoelectrode cross-sections were prepared with the use of a focused gallium ion beam (FIB, FEI Helios NanoLab 600 Dualbeam SEM/FIB) and the SEM photographs were realized at 3 kV. The transmission electron microscopy (TEM) was performed for the scrapped coatings on a JEOL 2100 operating at an accelerated voltage of 200 kV; it was also performed for photoelectrode cross-sections on an OSIRIS FEI that operated at 300 kV while coupled with an energy dispersive microscope. The solar cell performances were recorded on a Keithley model 2420 digital source meter under AM1.5G simulated sunlight (1000 $W·m^{-2}$).

3. Results and Discussion

Based on previous works carried out on the coating of Mo_6 or Ta_6 cluster-based compounds on TCO glass substrates (FTO or ITO),[52,71-74] the first part of this study is dedicated to the EPD of molybdenum iodide on FTO (CMI@FTO). The quality and the thickness of the coating prepared by EPD depend on i) the stability, the solvation state and the concentration of the dispersion solution, ii) the applied voltage which determines the generated current and thus the energy given to the particles in suspension and iii) the deposition time. More precisely, the resistance of the coating drives the deposition parameters, such as the voltage and the time. As the deposition of particles in suspension increases the resistance of the electrode, the electric current between the two immerged electrodes decreases until reaching a

8

limit, at which point the deposition stops. The energy given to the particles is no longer enough. Thus, a higher voltage for a suitable deposition time allows for obtaining a higher current, and therefore, thicker coatings. The aim was to optimize the EPD process (the nature of the solvent, the EPD parameters) for the preparation of forthcoming TSO-based photoelectrodes. For this, the impact on the film quality of the EPD solution and the deposition parameters (namely, the applied voltage and the deposition time) was studied. Three common solvents (ethanol, acetone and MEK) were selected as the dispersing media for the CMI compound to obtain orange/red, stable and transparent saturated solutions. From each suspension, orange/red, Mo_6 cluster iodide-based films (Figure S1 and 2a) were formed on the anode side, which is consistent with the negative charge of the anionic Mo_6-based cluster ($[Mo_6I^i_8I^a_6]^{2-}$ or the $[Mo_6I^i_8I^a_{6-z}(OH)^a_x(solvent)^a_y]^{n-}$ ($z = x + y$) species formed after an apical ligand exchange). It is worth noting that, as in previous studies,[52,71] for a similar thickness, the quality of CMI@FTO films (i.e., transparency and homogeneity) is higher when prepared from ketones, particularly from an acetone-based solution. This observation dictated our choice for acetone in the rest of this study. Then, the applied voltage, deposition time, and solution concentration were studied. The applied voltage appeared as the most impactful parameter. By increasing the voltage applied during the EPD process, the orange/red coloration of the Mo_6 films becomes more intense (Figure 2a): the thickness and the density of the Mo_6-based coatings increase and a red shift of the absorption threshold is noticed, but the transparency is not affected (Figure 2b). Above 20 V, the strength of coloration of the Mo_6 films tends toward that of the bulk (Figure 2a and 2c). This optical trend is similar for the films obtained from the solution that is weakly concentrated at 7 mM (Figure S2). However, the film transparency is then slightly lower with a transmittance of the most colored film around 65% (compared to 72% for the saturated solution). The impact of the deposition time is less visible (Figure S1b). Due to the high CMI concentration of the

9

saturated solution (17 mM), 5 s of deposition time is enough, in a voltage range from 10 V to 40 V, for obtaining strongly colored films. Finally, we selected for the study hereafter the acetone-based saturated solution as a deposition solution as well as a deposition time of 30 s. The microstructure and chemical composition of the films were studied using electron microscopy (SEM and TEM equipped with EDS, Figure 3), X-ray diffraction (XRD, Figure S3) and optical microscopy (Figure 4). The CMI@FTO films consist of a micrometric homogeneous amorphous layer of Mo_6 clusters. Indeed, the SEM photographs displayed in Figures 3a and 3b show a smooth, homogeneous and ~1 µm thick CMI coating on the FTO glass substrate. The TEM image and electron diffraction pattern in Figures 3c and 3d, as well as the XRD diagram (Figure S3), confirm the homogeneity of the film at a lower scale and highlight its real amorphous character. An atomic Mo/I ratio of 6/12 (theoretical value of 6/14) was estimated by EDS, which suggests a partial exchange of apical I^{-a} by solvent molecules or OH^- groups originating from acetone or water contamination. Moreover, Cs atoms were not clearly detectable, which is consistent with previous studies.[43,71-74] During the EPD process, due to their respective charge, the anionic Mo_6-based cluster nanoparticles and Cs^+ cations migrate at the opposite electrodes ; anionic Mo_6-clusters migrate toward the anode and Cs^+ go to the cathode side. Based on the published studies discussing the formation mechanism of molybdenum bromide-based films,[72,81] we assume the formation of a $[Mo_6I^i_8I^a_4(OH)^a_{2-x}(solvent)^a_x]^{n-}$ specie or more probably of the $[Mo_6I^i_8I^a_4(OH)^a_2]^{2-}$ anion, which generates $(H_3O)_2[Mo_6I^i_8I^a_4(OH)^a_2]$ then $[Mo_6I^i_8I^a_4(H_2O)^a_2].2H_2O$[82] coatings when the $[Mo_6I^i_8I^a_4(OH)^a_2]^{2-}$ anion is neutralized by H_3O^+ species (from the oxidation of contamination H_2O on the FTO electrode). Cracks are observed in the SEM images but cannot be detected with the naked eye. We suspect that they originated from the solvent evaporation after that EPD process or from the evaporation of adsorbed water molecules or the residual solvent under ultra-vacuum conditions during the SEM characterization. The optical microscopy

images in Figure 4 clearly show the appearance of the cracks by increasing the applied

voltage. Under 15 V, no crack is perceptible at the hundred-micrometer scale. Thus, the

cracks at high voltage could arise from the deposition kinetic (the higher the electric field, the

higher the kinetic) and the solvent evaporation, the impact of which increases with the coating

thickness (the larger concentration of solvent molecules, the more difficult the diffusion due

to a larger thickness). It is important to note here that the deposition of the Mo_6 cluster is

highly reproducible. For similar deposition conditions (the same EPD solution, applied

voltage and time), the evolution of the generated current is comparable and leads to films

having a similar thickness, microstructure and optical properties. Finally, the highest quality

crack-free CMI@FTO films were obtained at an applied voltage of 10 V for 30 s.

Indeed, homogeneous orange/red Mo_6 cluster iodide films with adjustable optical properties

have been prepared in a reproducible way by EPD on FTO substrates. After this proof of

concept, we investigated i) the realization of photoelectrodes (i.e., CMI@TSO@FTO with

TSO = TiO_2 or NiO) *via* the functionalization by the EPD process of nanostructured n- and p-

type TSO electrodes used in solar cell systems for energy conversion, namely TiO_2- and NiO-

based electrodes, and ii) the impact of the deposition method on photovoltaic performances.

As previously described, the mesoporous TiO_2 and NiO films were coated on FTO substrates

and CMI was deposited by the EPD method using the saturated acetone-based solution under

an applied voltage ranging from 2 V to 40 V for 30 s. As for the FTO substrate alone, a

homogeneous orange/red coloration occurs from 2 V, and its intensity increases in a

reproducible way with the voltage until reaching a strong red coloration for applied voltages

greater than 15 and 20 V for NiO and TiO_2, respectively (Figure 5). This suggests a good

surface coverage of TSO nanostructured films. Moreover, the CMI coating cannot be

removed even after a soaking in various solvents in which the cluster is soluble (ketone,

ethanol or dimethylformamide). This implies strong interactions between Mo_6 clusters and

11

TSO surfaces, and a real chemisorption phenomenon with a significant anchoring of clusters at the TSO surfaces. As shown in the photographs of Figure 5 and confirmed by the UV-vis transmittance spectra in Figure S4, the TiO_2-based films exhibit a high transparency with only a low decrease of transmittance (around 5%) with the film coloration. This trend is similar for the NiO-based films, although their transparency is lower. The chemical analyses and surface morphology were investigated with optical and electron microscopy (SEM and TEM). The morphology of the films turns out to be comparable to that of the mesoporous semiconducting films without clusters (Figure 5). The TSO surfaces are not covered with a dense amorphous CMI layer. The Mo_6 clusters seem to have penetrated the pores. This hypothesis is strengthened by the examination of SEM images and chemical analyses. Indeed, the cross-sections prepared with the focused ion beam (FIB) technique (Figures 6 and S5) show that the mesoporous morphology of TiO_2 and NiO films (around 1 μm thick) and the EDS analyses highlight i) the penetration of the Mo_6 cluster along the semiconductor films and ii) the presence of cesium in small amounts (determined ratio Mo/Cs from 6/0.2 to 6/0.6 compared to the theoretical value of 6/2). Moreover, the TEM images (inserts of Figure 5) show nanocrystallites surrounded by a thin amorphous cluster layer (around 1 – 3 nm corresponding to one to three cluster rows) confirming the homogeneous coating of TiO_2 and NiO by Mo_6 cluster species. The XRD patterns in Figure S3 corroborate the amorphous character of the CMI coating since the diffraction peaks correspond to the TSO layers only. As for the CMI@FTO films, the I/Mo atomic ratio determined by EDS on the CMI@TSO@FTO electrode surfaces is lower than the theoretical value, around 1.8 (1) and 2.0 (2) for the TiO_2 and NiO films, respectively. This is consistent with the apical ligand exchange described previously, namely $[Mo_6I^i_8I^a_{6-z}(OH)^a_x(solvent)^a_y]^{n-}$ species in solution. In light of our previous study on CMI@FTO, we investigated the crack process. Based on the optical microscope images (Figure 4), it seemed that, as for the CMI@FTO films, cracks appear on the NiO-

based films (CMI@NiO@FTO films) from an applied voltage of 20 V, whereas no crack is visible on the TiO_2-based films (CMI@TiO_2@FTO films) under the same conditions. This can be due to a difference of porosity and compactness between the two types of films. Indeed, we can see in Figures 5, 6 and S5 that the NiO films consist of conglomerates of NiO nanoparticles, whereas the spatial distribution of nanoparticles is better for TiO_2 electrodes (TiO_2 nanoparticles are better separated). It results in a non-uniform porosity for NiO films with larger pores corresponding to preferential flow paths of the charges in solution. Thus, the mesoporous network is weakened when the kinetic is too high, leading to cracks. Above 20 V, the electric field proves to be too large. It results in the damage of the NiO coating. Moreover, the SEM images on some of the TiO_2-based films that are prepared at 40 V highlight some breaks revealing the appearance of cracks (Figure S4b). Thus, in order to minimize the charge recombination and shunt currents, the photoelectrodes used for photovoltaic cell fabrication were prepared at 20 and 15 V for photoanodes (CMI@TiO_2@FTO) and photocathodes (CMI@NiO@FTO), respectively.

Compared to the previous study,[43] the photoelectrodes obtained by the EPD process rather than by the soaking method are in a reproducible way i) more homogeneous since no $Mo_6I_{14}(H_2O)_2 \cdot xH_2O$ micro-particles are observed and ii) more strongly colored (Figure S6). This higher film quality should result in higher photovoltaic performances. The solar cells were then assembled according to the vacuum back-filling technique.[79] The cells are noted as TiO_2/I, TiO_2/Co and NiO/Co for TSO/redox mediator. The cobalt electrolyte was preferred for the NiO-based cells for reasons of efficiency: the NiO/I cell obtained in a previous investigation[43] led to poor efficiency. In addition, cobalt electrolytes are known to lead to increased output potential for p-type solar cells, thanks to a drastically decreased charge recombination at the NiO/Dye interface, due to the steric bulk of the cobalt complex that limits interaction between holes in NiO and electrons on the redox mediator. The

performances of the solar cells under AM1.5 illumination (1000 W·m^{-2}) are depicted in Figure 7 and are gathered in Table 1; they are compared to those obtained from the soaking method. It is clearly evidenced that the photoconversion efficiency is systematically much higher by using EPD as the deposition process rather than the soaking method (Figure 7). It is important to note that the comparison of the best performances of the two types of cells is representative of all cell performances (the performances of the cells from photoelectrodes obtained from EPD are systematically higher). The improvement of the photoelectrode coloration leads to an increase of the short circuit current density (J_{SC}) by a factor of 2 or 3 for TiO$_2$- and NiO-based cells using iodide and cobalt electrolytes, respectively. In the case of the TiO$_2$ with a cobalt electrolyte (TiO$_2$/Co), an increase of the V$_{OC}$ is observed for EPD devices, in direct line with a better (denser) coverage of the surface of the semiconductor. However, the J$_{SC}$ is not improved despite the better light harvesting efficiency. This is likely due to steric effects: the cobalt complex diffusion in the electrolyte is sluggish and the regeneration of oxidized clusters (following photo-injection) is not favored from the kinetic point of view. However, due to the higher homogeneity of the film chemisorption and the decrease of the charge recombination (initially due to the microparticles of the condensed cluster on the semiconductor surface) the open circuit voltage (V$_{OC}$), the fill factor (FF), and the photoconversion efficiency (η) are clearly enhanced for all cells (Table 1). It is worth noting that, on one hand, the performances obtained here are comparable to those reported on solid state n-DSSCs based on a triarylamine organic dye functionalized by a carbazole unit.[83] On the other hand, the performances obtained for the NiO/Co system are also significant compared to those reported in recent works dealing with the investigation of Li-doped NiO in p-DSSC[84] or the use of novel carbazole-based push-pull organic dyes.[85] Indeed, the interfacial photo-induced charge separated state is rather long-lived. Cobalt redox shuttles can

only be implemented in p-type solar cells where the geminate charge recombination is slowed down, because the regeneration of the photo-reduced dye (or cluster in our case) is sluggish.

4. Conclusion

To sum up, orange/red transparent and homogeneous Mo_6 cluster iodide coatings on FTO glass substrates (CMI@FTO films) were prepared for the first time by the EPD process from a precursor solution of $Cs_2Mo_6I_{14}$. The EPD process (the solvent, the EPD parameters) was optimized and the optical properties, morphology and composition of the films were investigated. The coloration of the films can be, in a reproducible way, tuned by adjusting the deposition parameters (voltage and time). However, an important electric field leads to the generation of cracks. Then, the challenge in the preparation of cluster-based photoelectrodes consisted in obtaining homogeneous films with intense coloration and without cracks in order to have the best photovoltaic performances. By using EPD, we succeeded at fabricating high-quality, orange mesoporous photoanodes and photocathodes through the deposition of cluster-based, homogeneous, amorphous layers Mo_6 onto TiO_2 and NiO-based electrodes, respectively. This improvement of film quality compared to the classical soaking method led to the increase of the photoconversion efficiency of photovoltaic cells up to 300%. Beyond the DSSC cells, these promising results pave the way for the investigation of these homogeneous transition metal cluster-based surfaces for a panel of photoelectronic applications, ranging from photoelectrochemical devices (PEC) to all solid solar cells. The future challenges in using the Mo_6 cluster as a non-toxic alternative (stable under atmospheric conditions) to lead-halide perovskite is the realization of crystalline layers and the optimization of band alignment between the cluster and the n-type TSO in order to favor an effective charge transfer.[86]

Appendix A. Supplementary information is available in separate file.

References

[1]   B. O'Regan, M. Grätzel, A low-cost, high-efficiency solar cell based on dye-sensitized colloidal TiO_2 films, Nature 353 (1991) 737.

[2]   A. Fujishima, K. Honda, Electrochemical photolysis of water at a semiconductor electrode, Nature 238 (1972) 37.

[3]   Y. Cao, Y. Liu, S. M. Zakeeruddin, A. Hagfeldt, M. Grätzel, Direct contact of selective charge extraction layers enables high-efficiency molecular photovoltaics, Joule 2 (2018) 1108.

[4]   K. Kakiage, Y. Aoyama, T. Yano, K. Oya, J. Fujisawa, M. Hanaya, Highly-efficient dye-sensitized solar cells with collaborative sensitization by silyl-anchor and carboxy-anchor dyes, Chem. Commun. 51 (2015) 15894.

[5]   A Yella, H-W Lee, H N Tsao, C Yi, A K Chandiran, M K Nazeeruddin, E W-G Diau, C-Y Yeh, S M Zakeeruddin, M Grätzel, Porphyrin-sensitized solar cells with cobalt (II/III)–based redox electrolyte exceed 12 percent efficiency, Science 334 (2011) 629.

[6]   D. Lu, J. Li, G. Lu, L. Qin, D. Liu, P. Sun, F. Liu, G. Lu, Enhanced photovoltaic properties of dye-sensitized solar cells using three-component $CNF/TiO_2/Au$ heterostructure, J. Colloid and Interface Sci. 542 (2019) 168.

[7]   Y. Ding, J. Yao, L. Hu, S. Dai, Controlled synthesis of symbiotic structured TiO_2 microspheres to improve the performance of dye-sensitized solar cells, Sol. Energy 183 (2019) 587.

[8]   S. Powar, T. Daeneke, M. T. Ma, D. Fu, N. W. Duffy, G. Goetz, M. Weidelener, A. Mishra, P. Baeuerle, L. Spiccia, U. Bach, Highly efficient p-type dye-sensitized solar cells based on tris(1,2-diaminoethane)cobalt(II)/(III) electrolytes, Angew. Chem. Int. Ed. 52 (2013) 602.

[9]   A Renaud, B Chavillon, L Le Pleux, Y Pellegrin, E Blart, M Boujtita, T Pauporté, L. Cario, S Jobic, F Odobel, $CuGaO_2$: a promising alternative for NiO in p-type dye solar cells, J. Mater. Chem. 22 (2012) 14353.

[10]   A. J. Bard, M. A. Fox, Artificial photosynthesis: solar splitting of water to hydrogen and oxygen, Acc. Chem. Res. 28 (1995) 141.

[11]   R. Brimblecombe, A. Koo, G. C. Dismukes, G. F. Swiegers, L. Spiccia, Solar driven water oxidation by a bioinspired manganese molecular catalyst, J. Am. Chem. Soc. 132 (2010) 2892.

[12]   Z. Yu, F. Li, L. Sun, Recent advances in dye-sensitized photoelectrochemical cells for solar hydrogen production based on molecular components, Energy Environ. Sci. 8 (2015) 760.

[13]   N. Wei, Y. Liu, M. Feng, Z. Li, S. Chen, Y. Zheng, D. Wang, Controllable TiO_2 core-shell phase heterojunction for efficient photoelectrochemical water splitting under solar light, Appl. Catal. B Environ. 244 (2019) 519.

[14]   Q. Zhang, C. S. Dandeneau, X. Zhou, G. Cao, ZnO nanostructures for dye-sensitized solar cells, Adv. Mater. 21 (2009) 4087.

[15]   M. T. Efa, T. Imae, Effects of carbon dots on ZnO nanoparticle-based dye-sensitized solar cells. Electrochimica Acta 303 (2019) 204.

[16]   M. Wang, F. Ren, J. Zhou, G. Cai, L. Cai, Y. Hu, D. Wang, Y. Liu, L. Guo, S. Shen, N doping to ZnO nanorods for photoelectrochemical water splitting under visible light: engineered impurity distribution and terraced band structure, Scientific Reports 5 (2015) 12925.

[17]   J.-S. Yoon, J.-W. Lee, Y.-M. Sung, Enhanced photoelectrochemical properties of Z-scheme ZnO/p-n Cu_2O PV-PEC cells, J. Alloys Compd. 771 (2019) 869.

[18]   A. Tacca, L. Meda, G. Marra, A. Savoini, S. Caramori, V. Cristino, C. A. Bignozzi, V. G. Pedro, P. P. Boix, S. Gimenez, J. Bisquert, Photoanodes based on nanostructured WO_3 for water splitting, ChemPhysChem 13 (2012) 3025.

[19]   A. Apolinário, T. Lopes, C. Costa, J. P. Araùjo, A. M. Mendes, Multilayered WO_3 nanoplatelets for efficient photoelectrochemical water splitting: the role of the annealing ramp, ACS Appl. Energy Mater. 2 (2019) 1040.

[20]   H. Zheng, Y. Tachibana, K. Kalantar-zadeh, Dye-sensitized solar cells based on WO_3, Langmuir 26 (2010) 19148.

[21]   M. Younasa, M.A. Gondala, M.A. Dastageera, U. Baig, Fabrication of cost effective and efficient dye sensitized solar cells with WO_3-TiO_2 nanocomposites as photoanode and MWCNT as Pt-free counter electrode, Ceram. Int. 45 (2019) 936.

[22]   C.Hu, K. Chu, Y. Zhao, W. Y. Teoh, Efficient photoelectrochemical water splitting over anodized p-type NiO porous films, ACS Appl. Mater. Interfaces 6 (2014) 18558.

[23]   I. Yoo, S. S. Kalanur, H. Seo, A nanoscale p–n junction photoelectrode consisting of an NiO_x layer on aTiO$_2$/CdS nanorod core-shell structure for highly efficient solar water splitting, Appl. Catal. B Environ. 250 (2019) 200.

[24]   R. Tan, Z. Wei, J. Liang, Z. Lv, B. Chen, J. Qu, W. Yan, J. Ma, Enhanced open-circuit photovoltage and charge collection realized in pearl-like NiO/CuO composite nanowires based p-type dye sensitized solar cells, Mater. Res. Bull. 116 (2019) 131.

[25]   P. Wang, Y. H. Ng, R. Amal, Embedment of anodized p-type Cu_2O thin films with CuO nanowires for improvement in photoelectrochemical stability, Nanoscale 5 (2013) 2952.

[26]   Y. J. Jang, J. S. Lee, Photoelectrochemical water splitting with p-type metal oxide semiconductor photocathodes, ChemSusChem. 12 (2009) 1835.

[27]   J. Li, X. Jin, R. Li, Y. Zhao, X. Wang, X. Liu, H. Jiao, Copper oxide nanowires for efficient photoelectrochemical water splitting, Appl. Catal. B Environ. 240 (2019) 1.

[28]   T. Jiang, M. Bujoli-Doeuff, Y. Farré, Y. Pellegrin, E. Gautron, M. Boujtita, L. Cario, S. Jobic, F. Odobel, CuO nanomaterials for p-type dye-sensitized solar cells, RSC Adv. 6 (2016) 112765.

[29]   O. Langmar, E. Fazio, P. Schol, G. Torre, R. D. Costa, T. Torres, D. M. Guldi, Controlling interfacial charge transfer and fill factors in CuO-based tandem dye-Sensitized solar cells , Angew. Chem. Int. Ed. 58 (2019) 4056.

19

[30]   J. Gu, A. Wuttig, J. W. Krizan, Y. Hu, Z. M. Detweiler, R. J. Cava, A. B. Bocarsly, Mg-doped $CuFeO_2$ photocathodes for photoelectrochemical reduction of carbon dioxide, J. Phys. Chem. C 117 (2013) 12415.

[31]   L. Mao, S. Mohan, Y. Mao, Delafossite $CuMnO_2$ as an efficient bifunctional oxygen and hydrogen evolution reaction electrocatalyst for water splitting, J. Electrochem. Soc. 166 (2019) H233.

[32]   A. B. Muñoz-García, L. Caputo, E. Schiavo, C. Baiano, P. Maddalena, M. Pavone, Ab initio study of anchoring groups for $CuGaO_2$ delafossite-based p-type dye sensitized solar cells, Front. Chem. 7 (2019) 158.

[33]   I. C. Kaya, S. Akin, H. Akyildiz, S. Sonmezoglu, Highly efficient tandem photoelectrochemical solar cells using coumarin6 dye-sensitized $CuCrO_2$ delafossite oxide as photocathode, Sol. Energy, 169 (2018) 196.

[34]   A. Kojima, K. Teshima, Y. Shirai, T. Miyasaka, Organometal Halide Perovskites as Visible-Light Sensitizers for Photovoltaic Cells, J. Am. Chem. Soc. 131 (2009) 6050.

[35]   F. Bella, S. Galliano, G. Piana, G. Giacona, G. Viscardi, M. Grätzel, C. Barolo, C. Gerbaldi, Boosting the efficiency of aqueous solar cells: A photoelectrochemical estimation on the effectiveness of $TiCl_4$ treatment, Electrochim. Acta 302 (2019) 31.

[36]   M. Čolović, J. Volavšek, E. Stathatos, N. Č. Korošin, M. Šobak, I. Jerman, Amphiphilic POSS-based ionic liquid electrolyte additives as a boost for dye-sensitized solar cell performance, Sol. Energy 183 (2019) 619.

[37]   C. Li, C. Xin, L. Xu, Y. Zhong, W. Wu, Components control for high-voltage quasi-solid state dye-sensitized solar cells based on two-phase polymer gel electrolyte, Sol. Energy 181 (2019) 130.

[38]   P. Wang, L. Yang, , H. Wu, Y. Cao, J. Zhang, N. Xu, S. Chen, J.-D. Decoppet, S. M. Zakeeruddin, M. Grätzel, Stable and efficient organic dye-sensitized solar cell based on ionic liquid electrolyte, Joule 2 (2018) 2145.

[39]   V. Sundararajan, N. M. Saidi, S. Ramesh, K. Ramesh, G. Selvaraj, C. D. Wilfred, Quasi solid-state dye-sensitized solar cell with P(MMA-co-MAA)-based polymer electrolytes, J. Solid State Electrochem. 23 (2019) 1179.

[40]   F. Bella, M. Imperiyka, A. Ahmad, Photochemically produced quasi-linear copolymers for stable and efficient electrolytes in dye-sensitized solar cells, J. Photochem. Photobiol. A 289 (2014) 73.

[41]   M. Imperiyka, A. Ahmad, S. A. Hanifah, F. Bella, A UV-prepared linear polymer electrolyte membrane for dye-sensitized solar cells, Phys. B 450 (2014) 151.

[42]   B. Lee, Y. Ezhumalai, W. Lee, M.-C. Chen, C.-Y. Yeh, T. J. Marks, R. P. H. Chang, Cs_2SnI_6 encapsulated multi-dye sensitized all solid-state solar cells, ACS Appl. Mater. Interfaces, Just Accepted Manuscript, DOI: 10.1021/acsami.8b19778.

[43]   A. Renaud, F. Grasset, B. Dierre, T. Uchikoshi, N. Ohashi, T. Takei, A. Planchat, L. Cario, S. Jobic, F. Odobel, S. Cordier, Inorganic molybdenum clusters as light-harvester in all inorganic solar cells: A proof of concept, ChemistrySelect 1 (2016) 2284.

[44]   D. Bauer, H.-G. von Schnering, Beiträge zur chemie der elemente niob und tantal. LXVII. Die struktur der tantalhalogenide Ta_6Cl_{15} und Ta_6Br_{15}, Z. Anorg. Allg. Chem. 361 (1968) 259.

[45]   S. Cordier, C. Perrin, M. Sergent, Crystallochemistry of some new niobium bromides with (Nb_6Br_{18}) units: structures of $CsErNb_6Br_{18}$ and $Cs_2EuNb_6Br_{18}$, Z. Anorg. Allg. Chem. 619 (1993) 621.

21

[46]   S. Cordier, C. Loisel, C. Perrin, M. Sergent, Tantalum chlorides in octahedral cluster chemistry: the structures of $Cs_2PbTa_6Cl_{18}$ and $CsPbTa_6Cl_{18}$, J. Solid State Chem. 147 (1999) 350.

[47]   S. Kamiguchi, T. Mori, M. Watanabe, A. Suzuki, M. Kodomari, M. Nomurac, Y. Iwasawa, T. Chihara, Retention of the octahedral metal framework of Nb and Mo halide clusters in catalytic decomposition of phenyl acetate to phenol and ketene, J. Mol. Catal. A: Chem. 253 (2006) 176.

[48]   M. N. Sokolov, P. A. Abramov, M. A. Mikhailov, E. V. Peresypkina, A. V. Virovets, V. P. Fedin, Simplified synthesis and structural study of {Ta_6Br_{12}} clusters, Z. Anorg. Allg. Chem. 636 (2010) 1543.

[49]   J. König, I. Dartsch, A. Topp, E. Guillamón, R. Llusar, M. Köckerling, Air-stable, well-soluble $A^I_2[Nb_6Cl_{18}]$ cluster compounds (A^I = organic cation): a new route for preparation, single-crystal structures, properties, and ESI-mass spectra, Z. Anorg. Allg. Chem. 642 (2016) 572.

[50]   W. H. Chapin, Halide bases of tantalum, J. Am. Chem. Soc. 32 (1910) 323.

[51]   A. Renaud, M. Wilmet, T. G. Truong, M. Seze, P. Lemoine, N. Dumait, W. Chen, N. Saito, T. Ohsawa, T. Uchikoshi, N. Ohashi, S. Cordier, F. Grasset, Transparent tantalum cluster-based UV and IR blocking electrochromic devices, J. Mater. Chem. C 5 (2017) 8160 ;

[52]   T. K. N. Nguyen, A. Renaud, M. Wilmet, N. Dumait, S. Paofai, B. Dierre, W. Chen, N. Ohashi, S. Cordier, F. Grasset, T. Uchikoshi, New ultra-violet and near-infrared blocking filters for energy saving applications: fabrication of tantalum metal atom cluster-based nanocomposite thin films by electrophoretic deposition, J. Mater. Chem. C 5 (2017) 10477.

[53]   S. Nagashima, S. Kamiguchi, T. Chihara, Catalytic reactions over halide cluster complexes of group 5–7 metals, Metals 4 (2014) 235.

[54]   J. Löwe, D. Stock, B. Jap, P. Zwickl, W. Baumeister, R. Huber, Crystal structure of the 20S proteasome from the archaeon T. acidophilum at 3.4 A resolution, Science 268 (1995), 533.

[55]   P. Cramer, D. A. Bushnell, J. Fu, A. L. Gnatt, B. Maier-Davis, N. E. Thompson, R. R. Burgess, A. M. Edwards, P. R. David, R. D. Kornberg, Architecture of RNA polymerase II and implications for the transcription mechanism, Science 288 (2000) 640.

[56]   K. N. Ferreira, T. M. Iverson, K. Maghlaoui, J. Barber, S. Iwata, Architecture of the photosynthetic oxygen-evolving center, Science 303 (2004) 1831.

[57]   B. F. Mullan, M. T. Madsen, L. Messerle, V. Kolesnichenko, J. Kruger, X-ray attenuation coefficients of high-atomic-number, hexanuclear transition metal cluster compounds: A new paradigm for radiographic contrast agents, Acad. Radiol. 7 (2000) 254.

[58]   H.-T. Sun, Y. Sakka, Luminescent metal nanoclusters: controlled synthesis and functional applications, Sci. Technol. Adv. Mater. 15 (2014) 014205.

[59]   K. Costuas, A. Garreau, A. Bulou, B. Fontaine, J. Cuny, R. Gautier, M. Mortier, Y. Molard, J.-L. Duvail, E. Faulques, S. Cordier, Combined theoretical and time-resolved photoluminescence investigations of $[Mo_6Br^i_8Br^a_6]^{2-}$ metal cluster units: evidence of dual emission, Phys. Chem. Chem. Phys. 17 (2015) 28574.

[60]   B. Dierre, K. Costuas, N. Dumait, S. Paofai, M. Amela-Cortes, Y. Molard, F. Grasset, Y. Cho, K. Takahashi, N. Ohashi, T. Uchikoshi, S. Cordier, Mo_6 cluster-based compounds for energy conversion applications: comparative study of photoluminescence and cathodoluminescence, Sci. Technol. Adv. Mater. 18 (2017) 458.

[61]   J.-F. Dechézelles, T. Aubert, F. Grasset, S. Cordier, C. Barthou, C. Schwob, A. Maître, R. A. L. Vallée, H. Cramail, S. Ravaine, Fine tuning of emission through the engineering of colloidal crystals, Phys. Chem. Chem. Phys. 12 (2010) 11993.

[62] M. Turner, V.B. Golovko, O.P. Vaughan, P. Abdulkin, A. Berenguer-Murcia, M.S. Tikhov, B.F. Johnson, R.M. Lambert, Selective oxidation with dioxygen by gold nanoparticle catalysts derived from 55-atom clusters, Nature 454 (2008) 981.

[63] M. Feliz, M. Puche, P. Atienzar, P. Concepciun, S. Cordier, Y. Molard, In situ generation of active molybdenum octahedral clusters for photocatalytic hydrogen production from water, ChemSusChem 9 (2016) 1963.

[64] Y. Zhao, R. R. Lunt, Transparent luminescent solar concentrators for large-area solar windows enabled by massive Stokes-shift nanocluster phosphors, Adv. Ener. Mater. 3 (2013) 1143.

[65] A. Barras, M. R. Das, R. R. Devarapalli, M. V. Shelke, S. Cordier, S. Szunerits, R. Boukherroub, One-pot synthesis of gold nanoparticle/molybdenum cluster/graphene oxide nanocomposite and its photocatalytic activity, Appl. Catal. B 130 (2013) 270.

[66] P. S. Kuttipillai, Y. Zhao, C. J. Traverse, R. J. Staples, B. G. Levine, R. R. Lunt, Light-emitting diodes: Phosphorescent nanocluster light-emitting diodes, Adv. Mater. 28 (2016) 319.

[67] T. Aubert, F. Cabello Hurtado, M. A. Esnault, C. Neaime, D. Lebret-Chauvel, S. Jeanne, P. Pellen, C. Roiland, L. Le Polles, N. Saito, K. Kimoto, H. Haneda, N. Ohashi, F. Grasset, S. Cordier, Extended investigations on luminescent $Cs_2[Mo_6Br_{14}]@SiO_2$ nanoparticles: physico-structural characterizations and toxicity studies, J. Phys. Chem. C 117 (2013) 20154.

[68] K. Kirakci, V. Šícha, J. Holub, P. Kubàt, K. Lang, Luminescent hydrogel particles prepared by self-assembly of β-cyclodextrin polymer and octahedral molybdenum cluster complexes, Inorg. Chem. 53 (2014) 13012.

[69]   K. Kirakci, P. Kubàt, K. Fejfarova`, J. Martinčík, M. Nikl and K. Lang, X-ray inducible luminescence and singlet oxygen sensitization by an octahedral molybdenum cluster compound: a new class of nanoscintillators, Inorg. Chem. 55 (2016) 803.

[70]   C. Neaime, M. Amela-Cortes, F. Grasset, Y. Molard, S. Cordier, B. Dierre, M. Mortier, T. Takei, K. Takahashi, H. Haneda, M. Verelst, S. Lechevallier, Time-gated luminescence bioimaging with new luminescent nanocolloids based on $[Mo_6I_8(C_2F_5COO)_6]^{2-}$ metal atom clusters, Phys. Chem. Chem. Phys. 18 (2016) 30166.

[71]   T. K. N. Nguyen, F. Grasset, B. Dierre, C. Matsunaga, S. Cordier, P. Lemoine, N. Ohashi, T. Uchikoshi, Fabrication of transparent thin film of octahedral molybdenum metal clusters by electrophoretic deposition, ECS J. Solid State Sci. Technol. 5 (2016) R178.

[72]   T. K. N. Nguyen, B. Dierre, F. Grasset, A. Renaud, S. Cordier, P. Lemoine, N. Ohashi, T. Uchikoshi, Formation mechanism of transparent Mo_6 metal atom cluster film prepared by electrophoretic deposition, J. Electrochem. Soc. 164 (2017) D412.

[73]   T. K. N. Nguyen, B. Dierre, F. Grasset, N. Dumait, S. Cordier, P. Lemoine, A. Renaud, H. Fudouzi, N. Ohashi, T. Uchikoshi, Electrophoretic coating of octahedral molybdenum metal clusters for UV/NIR light screening, Coatings 7 (2017) 114.

[74]   T. K. N. Nguyen, A. Renaud, B. Dierre, B. Bouteille, M. Wilmet, M. Dubernet, N. Ohashi, F. Grasset, T. Uchikoshi, Extended study on electrophoretic deposition process of inorganic octahedral metal clusters: advanced multifunctional transparent nanocomposite thin films, Bull. Chem. Soc. Jpn. 91 (2018) 1763.

[75]   K. Kirakci, S. Cordier, C. Perrin, Synthesis and characterization of $Cs_2Mo_6X_{14}$ (X = Br or I) hexamolybdenum cluster halides: efficient Mo_6 cluster precursors for solution chemistry syntheses, Z. Anorg. Allg. Chem. 631 (2005) 411.

[76]   J. Warnan, Y. Pellegrin, E. Blart, F. Odobel, Supramolecular light harvesting antennas to enhance absorption cross-section in dye-sensitized solar cells, Chem. Commun. 48 (2012) 675.

[77]   A. Nattestad, A. J. Mozer, M. K. R. Fischer, Y.-B. Cheng, A. Mishra, P. Bäuerle, U. Bach, Highly efficient photocathodes for dye-sensitized tandem solar cells, Nat. Mater. 9 (2010) 31.

[78]   A. Renaud, B. Chavillon, L. Cario, L. Le Pleux, N. Szuwarski, Y. Pellegrin, E. Blart, E. Gautron, F. Odobel, S. Jobic, Origin of the Black Color of NiO Used as Photocathode in p-Type Dye-Sensitized Solar Cells, J. Phys. Chem. 117 (2013) 22478.

[79]   A. Nattestad, M. Ferguson, R. Kerr, Y.-B. Cheng, U. Bach, Dye-sensitized nickel(II) oxide photocathodes for tandem solar cell applications, Nanotechnology 19 (2008) 295304/1.

[80]   E. A. Gibson, A. L. Smeigh, L. Le Pleux, L. Hammarström, F. Odobel, G. Boschloo, A. Hagfeldt, J. Phys. Chem. C 115 (2011) 9772.

[81]   L. J. Guggenberger, A. W. Sleight, Structural and bonding characterizations of molybdenum dibromide, $Mo_6Br_{12}.2H_2O$, Inorg. Chem. 8 (1969) 2041.

[82]   H. Schafer, B. Plautz, H. Plautz, Die dihydrate $[Me_6X_8^i]X_4^a \cdot 2H_2O$ mit Me = Mo, W; X = Cl, Br, J, Z. anorg. allg. Chem. 389 (1972) 57.

[83]   A. Delices, J. Zhang, M.-P. Santoni, C.-Z. Dong, F. Maurel, N. Vlachopoulos, A. Hagfeldt, M. Jouini, New covalently bonded dye/hole transporting material for better charge transfer in solid-state dye-sensitized solar cells, Electrochimica Acta 269 (2018) 163.

[84]   L. Wei, L. Jiang, S. Yuan, X. Ren, Y. Zhao, Z. Wang, M. Zhang, L. Shi, D. Li, Valence band edge shifts and charge-transfer dynamics in Li-doped NiO based p-type DSSCs, Electrochimica Acta 188 (2016) 309.

[85]   A. Carella, R. Centore, F. Borbone, M. Toscanesi, M. Trifuoggi, F. Bella, C. Gerbaldi, S. Galliano, E. Schiavo, A. Massaro, A. B. Muñoz-García, M. Pavone, Tuning optical and

electronic properties in novel carbazole photosensitizers for p-type dye-sensitized solar cells,

Electrochimica Acta 292 (2018) 805.

[86]   J. P. C. Baena, L. Steier, W. Tress, M. Saliba, S. Neutzner, T. Matsui, F. Giordano, T.

J. Jacobsson, A. R. S. Kandada, S. M. Zakeeruddin, A. Petrozza, A. Abate, M. K.

Nazeeruddin, M. Grätzel, A. Hagfeldt, Highly efficient planar perovskite solar cells through

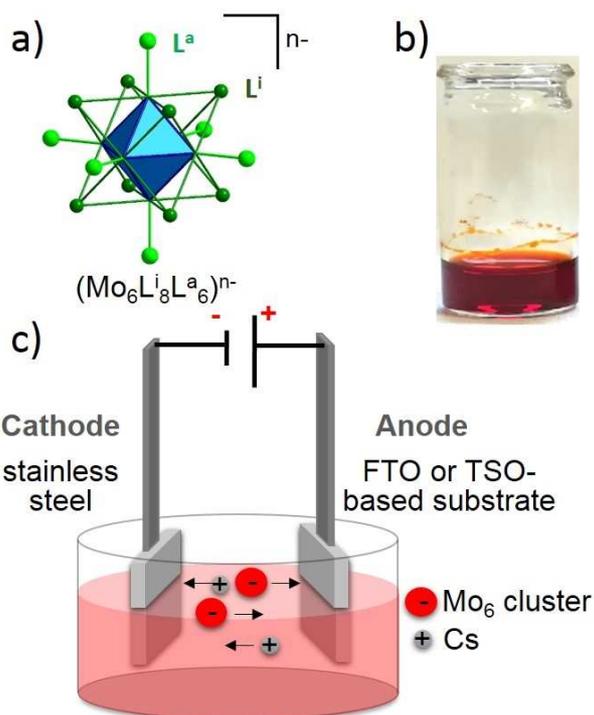band alignment engineering, Energy Environ. Sci. 8 (2015) 2928.

Fig. 1. *a) Representation of the Mo$_6$ cluster anion; L^i and L^a correspond to inner and apical ligands, respectively. b) Photograph of the acetone-based saturated deposition solution and c) schematic representation of the EPD setup.*
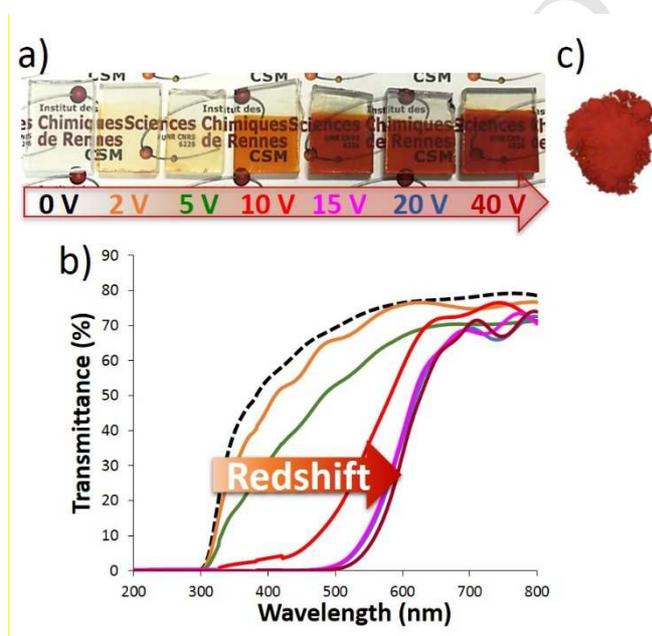
Fig. 2. *a) Photographs of the colored CMI@FTO films obtained from the acetone-based saturated deposition solution (17 mM) at various applied voltages during 30 s and b) their UV-vis transmission spectra. c) Photograph of the CMI powder.*
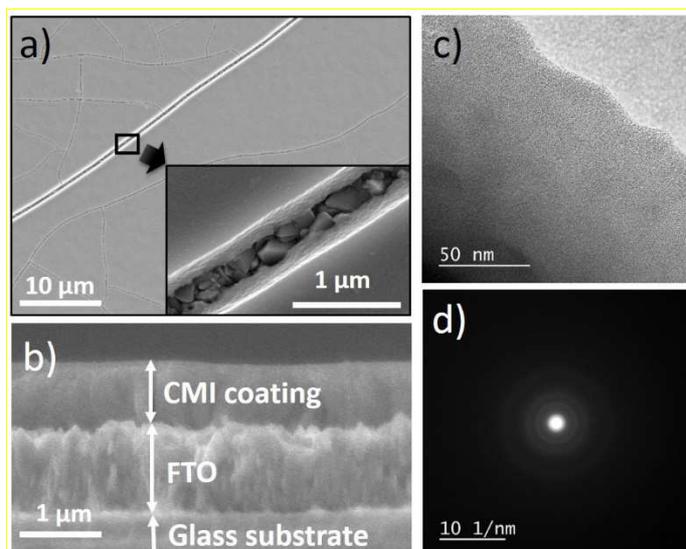
Fig. 3. *a) and b) SEM images of the surface and the cross section of a CMI@FTO film prepared by EPD with the deposition solution at a concentration of 17 mM at 10 V for 30 s. TEM c) image and d) diffraction pattern of the scrapped film.*
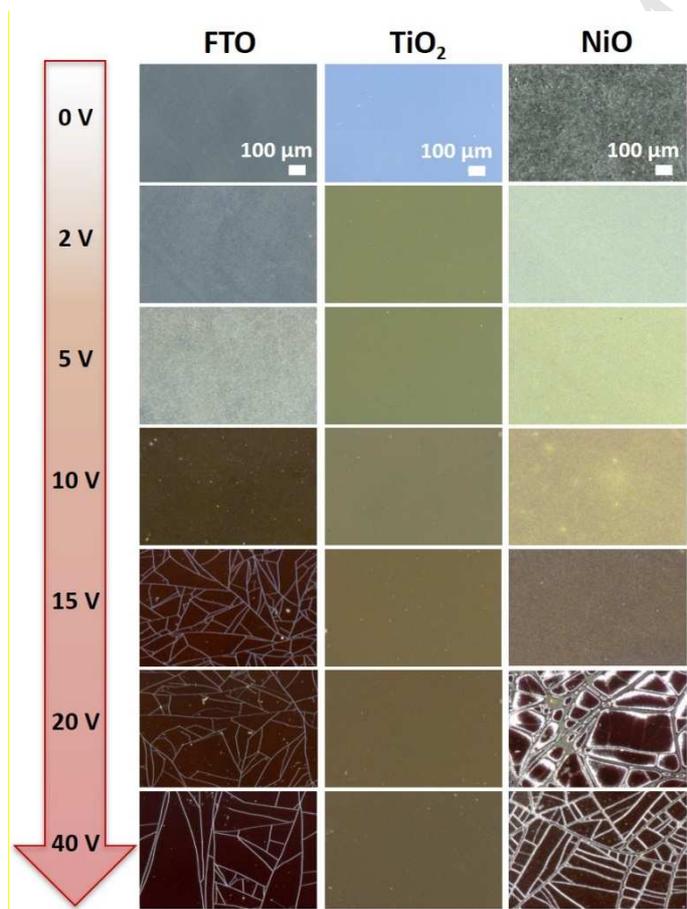
Fig. 4. Optical microscopy photographs of CMI films on FTO substrate (CMI@FTO), TiO$_2$ (CMI@TiO$_2$@FTO) and NiO (CMI@NiO@FTO) electrodes according the applied voltage.
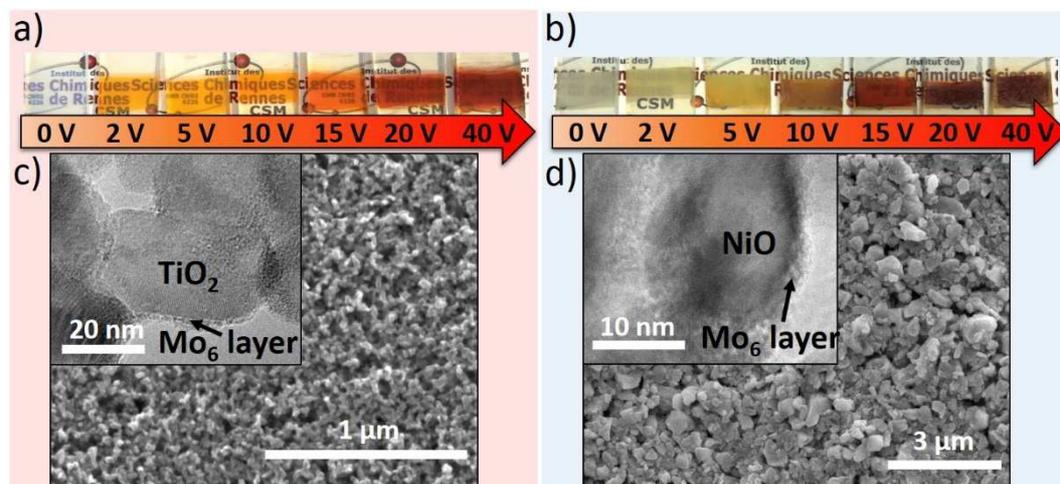

Fig. 5. Photographs of a) CMI@TiO$_2$@FTO and b) CMI@NiO@FTO photoelectrodes prepared by doctor blading before and after coloration by EPD with the CMI deposition solution of 17 mM at different voltages for 30 s. SEM and TEM (insert) of b) CMI@TiO$_2$@FTO and c) CMI@NiO@FTO photoelectrodes prepared at 20 V and 15 V for 30 s respectively.
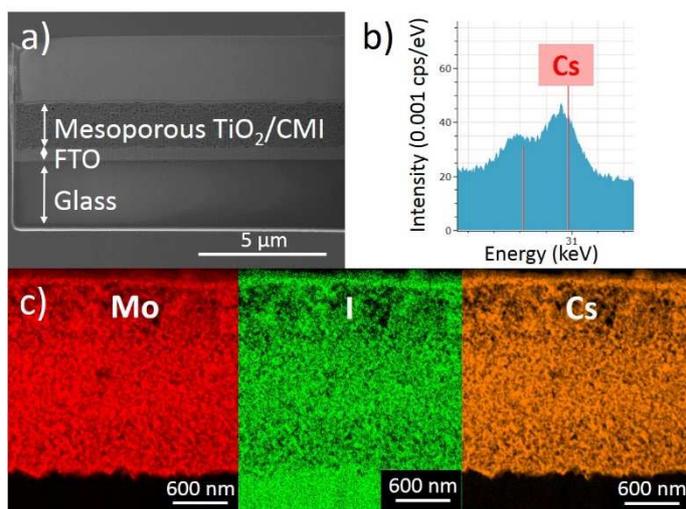

Fig. 6. a) SEM image of a cross-section a CMI@TiO$_2$@FTO photoelectrode obtained at 20 V for 30 s and b) and c) EDS analyses on the mesoporous TiO$_2$/CMI layer. Iodine and tin rays

are detected in the same energy range and cannot be separated explaining an error of
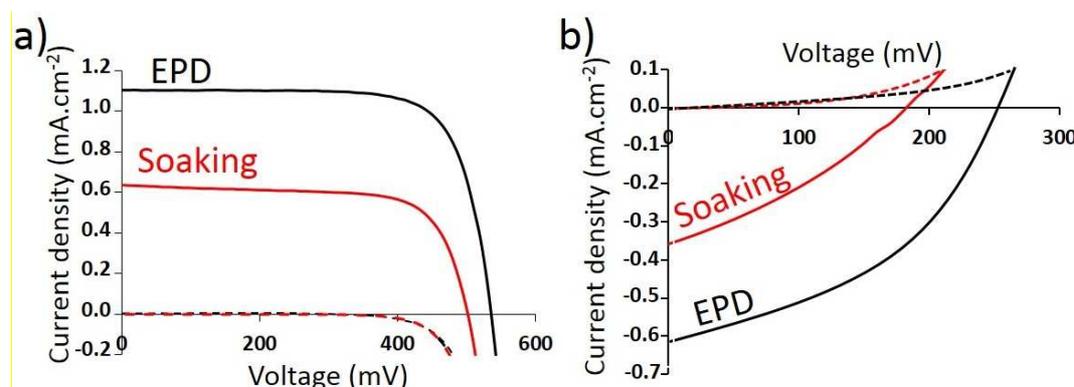
detection of I in the FTO layer.

Fig. 7. *Comparison of photoresponses in the dark (dash lines) and underAM$_{1.5}$ illumination*

(1000 W·m^{-2}, solid line) of photovoltaic cells prepared from a) CMI@TiO$_2$@FTO and b)

CMI@NiO@FTO photoelectrodes colored by soaking method or by EPD for 30 s at 20 and

15 V, respectively. The electrolytes used were the I$^-$/I$_3^-$ couple and the cobalt complex for a)

CMI@TiO$_2$@FTO and b) CMI@NiO@FTO photoelectrodes, respectively.

Table 1. *Photovoltaic performances of DSC devices constructed with TiO$_2$ and NiO as n- and*

p-type semiconductors deposited by EPD or in parentheses by soaking method.

TSO-electrolyte	J_{SC} (mA·cm^{-2})	V_{OC} (mV)	FF (%)	η (%)
TiO$_2$-I	1.13 (0.64)	529 (502)	74 (71)	0.44 (0.23)
TiO$_2$-Co	0.90 (1.17)	371 (295)	75 (54)	0.25 (0.19)
NiO-Co	0.61 (0.36)	254 (183)	43 (32)	0.07 (0.02)